A Journal of the Gesellschaft Deutscher Chemiker

Angewandte International Edition GDCh Chemie

www.angewandte.org

Accepted Article

Title: On-surface Synthesis of Triaza[5]triangulene through Cyclodehydrogenation and its Magnetism

Authors: Donglin Li, Orlando J. Silveira, Takuma Matsuda, Hironobu Hayashi, Hiromitsu Maeda, Adam S. Foster, and Shigeki Kawai

To be cited as: *Angew. Chem. Int. Ed.* **2024**, e202411893

Link to VoR: https://doi.org/10.1002/anie.202411893

WILEY VCH

10.1002/anie.202411893

WILEY VCH

RESEARCH ARTICLE

On-surface Synthesis of Triaza[5]triangulene through Cyclodehydrogenation and its Magnetism

Donglin Li[a], Orlando J. Silveira[b], Takuma Matsuda[c], Hironobu Hayashi[a], Hiromitsu Maeda*[c], Adam S. Foster*[b],[d], Shigeki Kawai*[a],[e]

[a] Dr. D. Li, Dr. H. Hayashi, Prof. Dr. S. Kawai
Center for Basic Research on Materials
National Institute for Materials Science
Tsukuba 305-0047 (Japan)
E-mail: KAWAI.Shigeki@nims.go.jp

[b] Dr. O. J. Silveira, Prof. Dr. A. S. Foster
Department of Applied Physics
Aalto University
P.O. Box 11100, Aalto, Espoo 00076 (Finland)
E-mail: adam.foster@aalto.fi

[c] T. Matsuda, Prof. Dr. H. Maeda
Department of Applied Chemistry, College of Life Sciences
Ritsumeikan University
Kusatsu 525-8577 (Japan)
E-mail: maedahir@ph.ritsumei.ac.jp

[d] Prof. Dr. A. S. Foster
Nano Life Science Institute (WPI-NanoLSI)
Kanazawa University
Kanazawa 920-1192 (Japan)

[e] Prof. Dr. S. Kawai
Graduate School of Pure and Applied Sciences,
University of Tsukuba
Tsukuba 305-8571 (Japan)

Abstract: Triangulenes as neutral radicals are becoming promising candidates for future applications such as spintronics and quantum technologies. To extend the potential of the advanced materials, it is of importance to control their electronic and magnetic properties by multiple graphitic nitrogen doping. Here, we synthesize triaza[5]triangulene on Au(111) by cyclodehydrogenation, and its derivatives by cleaving C–N bonds. Bond-resolved scanning tunneling microscopy and scanning tunneling spectroscopy provided detailed structural information and evidence for open-shell singlet ground state. The antiferromagnetic arrangement of the spins in positively doped triaza[5]triangulene was further confirmed by density function theory calculations. The key aspect of triangulenes with multiple graphitic nitrogen is the extra p_z electrons composing the π orbitals, favoring charge transfer to the substrate and changing their low-energy excitations. Our findings pave the way for the exploration of exotic low-dimensional quantum phases of matter in heteroatom doped organic systems.

Introduction

A unique class of open-shell nanographene, the zigzag-edged triangular nanographene, has attracted enormous interest as a promising candidate in next-generation molecular spintronics due to their multiple unpaired π-electrons and intriguing magnetic properties.[1] However, the high reactivity of the zigzag edge leads to a long-standing challenge to synthesize unsubstituted triangulenes in solution based organic chemistry. In this regard, on-surface synthesis[2] has become a powerful strategy to fabricate triangulenes under ultra-high vacuum conditions because such reactive carbon-based structures can be obtained from designer precursors. So far, a series of triangulenes have been synthesized on surfaces by both tip-induced manipulation[3] and annealing of precursors.[4] The previous studies demonstrated that the total net spin of triangulene and its higher homologues ($N \geq 3$, where N is the number of carbon atoms on each zigzag edge) linearly increases with their size N (Scheme 1a). However, even using the on-surface synthesis strategy, extended triangulenes ($N > 7$) with higher polyradicals poses significant challenges in terms of the solubility of the precursors and the thermal stability during sublimation. It has been demonstrated that heteroatom doping of graphene-based structures allows further tuning of their electronic and magnetic properties.[5] For instance, introducing a nitrogen atom into the triangulene structure is an alternative approach to obtain a higher polyradical, consequently inducing an additional π-electron to the triangulene due to the double occupancy of the nitrogen's p_z orbital.[5d,6] The introduction of more nitrogen atoms into the same sublattice sites increases the imbalance of the π-electrons, which in a controlled scenario can be used as a tool to tailor the magnetism that arises from the topological frustrations.

Here, we successfully synthesized triaza[5]triangulene (**2**), a version of the $N = 5$ triangulene with three graphitic nitrogen atoms, in which the spin and orbital degeneracy coexist, driving

10.1002/anie.202411893

the molecule to a valley-mixing phase in its neutral phase. We synthesized **2** from 4,8,12-Tris(2,6-dimethylphenyl)-4,8,12-triazatriangulenium^{+}-Cl^{-} (**1**) as a precursor ion pair by cyclodehydrogenation on the Au(111) surface (Scheme 1b). Surprisingly, C–N bonds in **1** were also broken during the annealing process, resulting in the additional formation of N-doped trapezoidal nanographene (**3**) and triaza[3]triangulene (**4**), in which pyridinic nitrogen atoms exist. A combination of bond-resolved scanning tunneling microscopy (BR-STM) with a carbon monoxide (CO) terminated tip[7] and scanning tunneling spectroscopy (STS) revealed that all three products exhibit an open-shell singlet ground state on Au(111). Our density function theory (DFT) calculations show an S = 1/2 state in gas-phase neutral **2** and **3**, suggesting that the open shell-singlet is a consequence of charge transfer between molecule and substrate. This is consistent with cationic versions of **2** and **3** with antiferromagnetic (AF) alignment. Hence, the excitation of two exchange coupled spins by tunneling electrons is the reason for the symmetric steps around the Fermi level observed in the STS, where the magnetic exchange coupling (MEC) strengths in **2**, **3**, and **4** are 9, 10.6, and 31 meV, respectively. Our finding validates the influence of multiple graphitic nitrogen doping on high-spin nanographene.

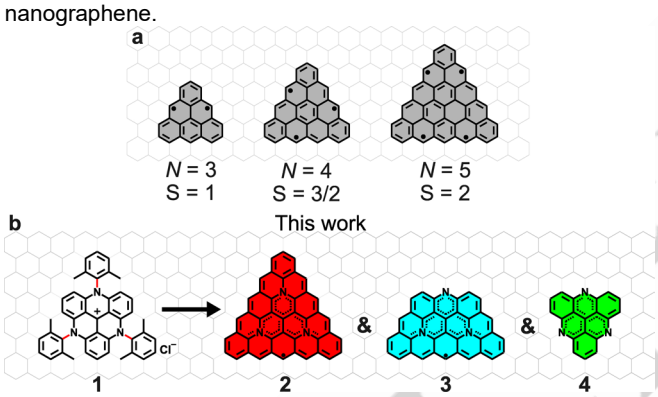

Scheme 1. Chemical structures of open-shell triangulenes and synthesis strategy for azatriangulenes and nitrogen-doped nanographene. (a) Triangulenes with different numbers of zigzag carbon atoms (*N*) and predicted spin multiplicity (S), having a linear relationship between S and *N*. (b) Chemical structures of 4,8,12-Tris(2,6-dimethylphenyl)-4,8,12-triazatriangulenium^{+}-Cl^{-} (**1**) as a precursor ion pair and triaza[5]triangulene (**2**), nitrogen-doped nanographene (**3**), and triaza[3]triangulene (**4**) as products. C–N bonds indicated by red lines in **1** can be broken during cyclodehydrogenation. The N–H bonds in **3** and **4** are omitted for simplicity.

Results and Discussion

The precursor **1** was synthesized via solution chemistry (see Supporting Information for detailed synthetic procedures). To obtain triaza[5]triangulene, several different preparation parameters were tested. For example, **1** was either deposited on Au(111) kept at room temperature followed by annealing the sample to 300 °C or deposited on Au(111) kept at elevated temperatures (300~400 °C). We found that increasing the substrate temperature increased the reaction yield of triaza[5]triangulene. The products were finally obtained by depositing **1** on Au(111) kept at 380 °C (Figure S1) and subsequently were characterized with STM at 4.3 K. We observed three kinds of isolated products as indicated by squares in red, blue, and green (Figure 1a), with yields of 5%, 13%, and 3%, respectively (Figure S2). The close-up view of the STM topography in the area indicated by the red square shows the product as an equilateral triangular shape with a side length of approximately 1.4 nm (Figure 1b). Both the shape and side length are consistent with those of triaza[5]triangulene. Next, the close-up view of the STM topography in the area indicated by the blue square shows an isosceles trapezoid shaped molecule (Figure 1c). The length of the longer side was approximately 1.4 nm, which is almost identical to the side length of **2**. Therefore, we tentatively identify this molecule as a broken triaza[5]triangulene, which is formed by accidental cleavage of one C–N bond during the cyclodehydrogenation process. Additionally, we observed a molecule with a smaller equilateral triangular shape as indicated by the green square (Figure 1d). The side length is approximately 0.9 nm, which is smaller than that of triaza[5]triangulene (Figure 1b). This molecule is likely triaza[3]triangulene, formed by dissociating all dimethylphenyl groups during the cyclodehydrogenation. The constant-height BR-STM image (Figure 1e) of the larger triangular molecule and the corresponding Laplace filtered image (Figure 1f) reveal the skeletal structure. However, the left corner part was still unclear. By setting the tip closer to the surface by 21 pm, the hexagonal ring appeared at the corner (Figure S3), meaning that the molecule was composed of 15 fused six-membered rings. Thus, the larger triangular molecule corresponds to **2**. The neutral form of **2** was tentatively depicted in Figure 1g, which helped to identify the number of its π-electrons as 49. We found significant variations of the contrasts at the edges of **2** in the BR-STM image. The bright contrast around the edge should relate to the spin polarization.[8] Note that no significant feature relating to the CH_2 termination caused by imperfect cyclodehydrogenation was observed.[9] The BR-STM image (Figure 1h) of the trapezoidal molecule and the corresponding Laplace-filtered image (Figure 1i) show 12 fused six-membered rings in the molecule. Thus, the product was synthesized via cyclodehydrogenation among two 2,6–dimethylphenyl groups and the triaza[3]triangulene core while the last phenyl group was simply dissociated, that is **3** (Figure 1j). After this dissociation, the N atom at the edge was passivated by an H atom, as demonstrated by the manipulation experiment (Figure S4). The BR-STM image (Figure 1k) of the smaller triangular molecule and the corresponding Laplace filtered image (Figure 1l) show three benzene rings and a darker region at the center. Due to the high mobility of this small molecule, it was challenging to obtain a higher resolution image. Inspired by the formation of **3**, this smaller molecule could correspond to **4**, which was synthesized via dissociation of three 2,6-dimethylphenyl groups in **1** (Figure 1m). This compound deviates from our main focus due to the absence of the graphitic nitrogen doping. Moreover, substituting CH groups at zigzag edges with N atoms can retain the electronic properties of the molecule because the nitrogen atom maintains the π-system topology equivalent to that of the substituted CH group.[10] Additionally, the

10.1002/anie.202411893

RESEARCH ARTICLE

contribution of such pyridinic nitrogen to the modulation of the magnetic property is considerably less.[11] Therefore, we focus on the products with graphitic nitrogen atoms, **2** and **3**. Apart from the isolated products, a number of dimers and trimers as well as oligomers of **2**–**4** were also formed because the highly reactive edges of open-shell molecules tend to be stabilized by fusing with each other at elevated temperatures.[12] In a fused product composed of one **3** and two **4** molecules, **4** was bound to the longer side of **3** (Figure S5). The reactivity of the longer side is most probably higher than that of the shorter one due to the localized spins. Note that we found absence of the product synthesized by dissociating two 2,6-dimethylphenyl groups from **1**, most probably relating to the low cleavage barrier of the last C–N bond.

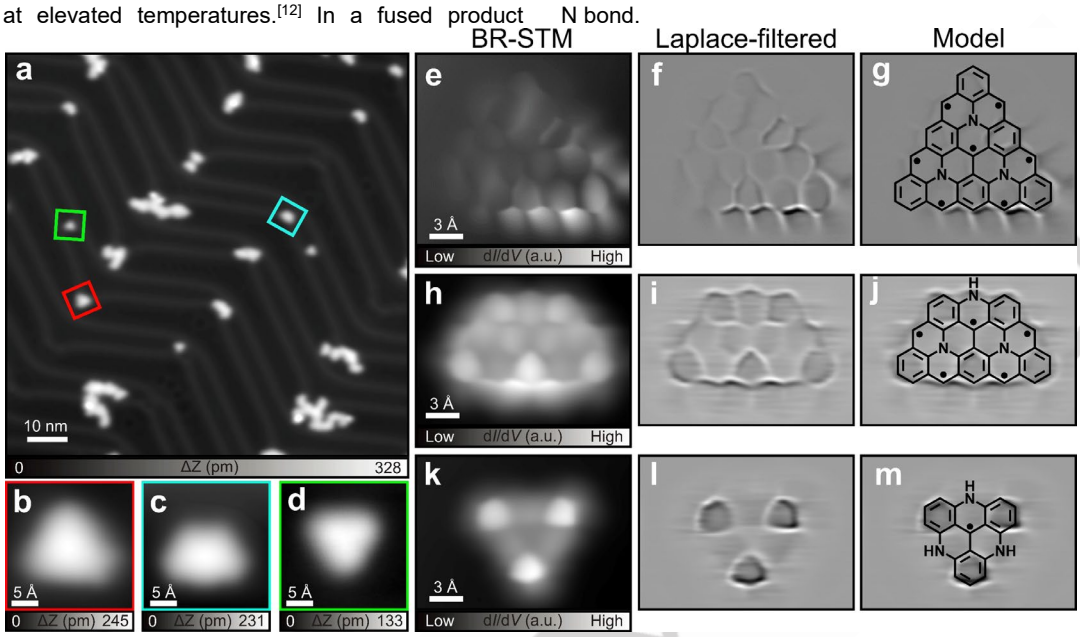

Figure 1. On-surface syntheses of **2**–**4**. (a) Large-scale STM image of the sample prepared by depositing precursor **1** on Au(111) kept at 380 °C. (b–d) Close-up views of **2**, **3**, and **4**, respectively. (e, h, k) BR-STM images over the structure in (b–d), (f, i, l) the corresponding Laplace filtered images, and (g, j, m) the chemical structures superimposed on the corresponding Laplace filtered images. Measurement parameters: sample bias voltage V = 200 mV and tunneling current I = 10 pA in (a). V = 200 mV and I = 10 pA in (b). V = 200 mV and I = 2 pA in (c). V = 100 mV and I = 10 pA in (d).

Ovchinnikov's rule[13] and Lieb's theorem[14] are commonly employed to estimate the spin state of [*N*]triangulenes.[15] However, we found that the products do not follow the Ovchinnikov-Lieb rules since the system does not obey half-filling, complicating the prediction of their ground state. We investigated magnetic properties of **2** and **3** by acquiring low energy d*I*/d*V* spectra (Figure 2). Both d*I*/d*V* curves (middle panels in Figure 2) show dip features at the zero bias surrounded by two symmetric steps, which are attributed to excitation by tunneling electrons of spins localized at different sites in molecules.[16] This is consistent with the distinct contrasts observed by BR-STM as shown in Figure 1, where brighter spots are observed at the corner and edge of **2** and at the larger edge of **3**. Assuming the spins are concentrated over these brighter areas, the tunneling electrons can inelastically flip the spins through a resonance process when the energy is equivalent to the exchange coupling between the spins.[17] We assume that the p_z electrons modified by the nitrogen atom doping induce spin alignment in the system and act as apparent sublattices localized at the bright spots in Figure 1. The absence of Kondo resonance at the zero bias in the d*I*/d*V* curves indicates a spin-flipping transition from open-shell singlet states to triplets, which is similar to an AF to ferromagnetic (FM) transition.[18] Since **2** and **3** with the geometries proposed here contain odd numbers of electrons, only a charge transfer mechanism between the products and the underlying gold substrate could influence their spin multiplicity in a way that allows such spin states.[5d] Electron donation to gold surfaces is expected in nitrogen-functionalized systems due to the misalignment of their Fermi level with the vacuum.[19] The corresponding inelastic electron tunneling spectroscopy (IETS) spectrum of **2** shows that the MEC between spins is ~9 meV while that of **3** shows a similar MEC of 10.6 meV (right panels in Figure 2). Note that **4** has an MEC energy of 31 meV (Figure S6), which is relatively large for [3]triangulene-based structures.[20] We also measured the fused trimer composed of one **3** and two **4** molecules and the measured MEC energy (9.6 mV) over the **4** unit in the fused molecule was smaller than that of the isolated **4** (Figure S5). The strong spin coupling between multi spin units significantly reduces the energy difference between the ground state and the excited state of **4**.

10.1002/anie.202411893
WILEY VCH

RESEARCH ARTICLE

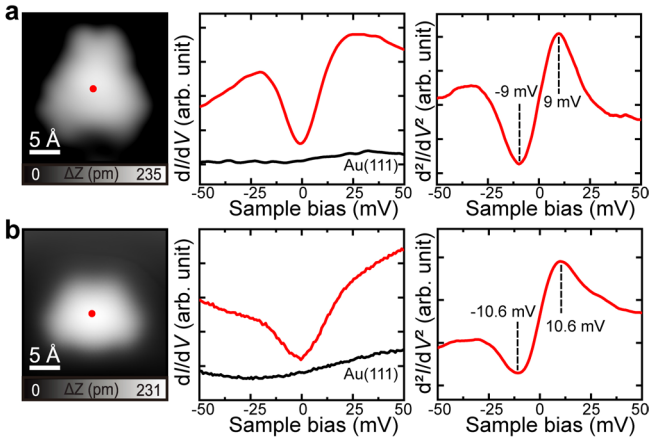

Figure 2. Characterization of the magnetic properties of **2** and **3**. (a, b) d*I*/d*V* and IETS spectra were taken at the sites marked by red dots in the left panel in a and b, respectively. V_{ac} = 5 mV. The d*I*/d*V* curves in black were taken over the bare Au(111) surface.

To get an insight into the spin state of the products and to elucidate the charge transfer mechanism, we investigated their frontier orbitals using STS measurements. The d*I*/d*V* spectra taken at three different sites of **2** have several electronic resonances at 0.9, −0.9, and −1.3 V as well as a dip feature around the Fermi level (Figure 3a). We found that the contrasts in the constant current d*I*/d*V* maps at the corresponding energies are C_2 symmetric rather than C_3 symmetric (Figure 3b). The spatial distributions of the d*I*/d*V* maps measured at −0.9 and 0.9 V concentrated along the edges, with the number of bright lobes matching those in the simulated maps at −1.2 and 0.9 V, respectively (Figure 3c). Thus, the energies relate to the DFT frontier orbitals ψ_4 and ψ_3 in Figure 3d.[5d] Here, we selected the energies of the simulated images to get a best agreement with the measured d*I*/d*V* maps. The simulated d*I*/d*V* maps (Figure S7) over a wider energy range reveal significant broadening of the corresponding orbitals (Figure 3e). The orbitals ψ_2 and ψ_3 have similar distributions as the d*I*/d*V* images measured at −0.7 to −1.1 V have similar contrasts (Figure S8). We also found that the d*I*/d*V* image at −1.3 V (Figure 3b) is in agreement with the simulated d*I*/d*V* map at −1.8 V, corresponding to the ψ_1 orbital. It should be noted that the slight deviation of the energies would relate to the hybridization of the molecular orbitals with the substrate. The energy levels in Figure 3e reveal the open-shell characteristic of $\mathbf{2}^+$, where the low energy spin orbitals are degenerated but spatially separated (for example, both spin orbitals of ψ_1 are at the same energy (Figure 3e) but are located at opposite sides of $\mathbf{2}^+$ (Figure 3d)). Note that charging the molecule leaves the ψ_4 orbital unoccupied, breaking the orbital-degeneracy observed in neutral **2**. The d*I*/d*V* maps of **3** and **4** were also measured at different energies (Figures S9,S10). We found that **4** was highly mobile at negative sample bias voltages (Figure S11).

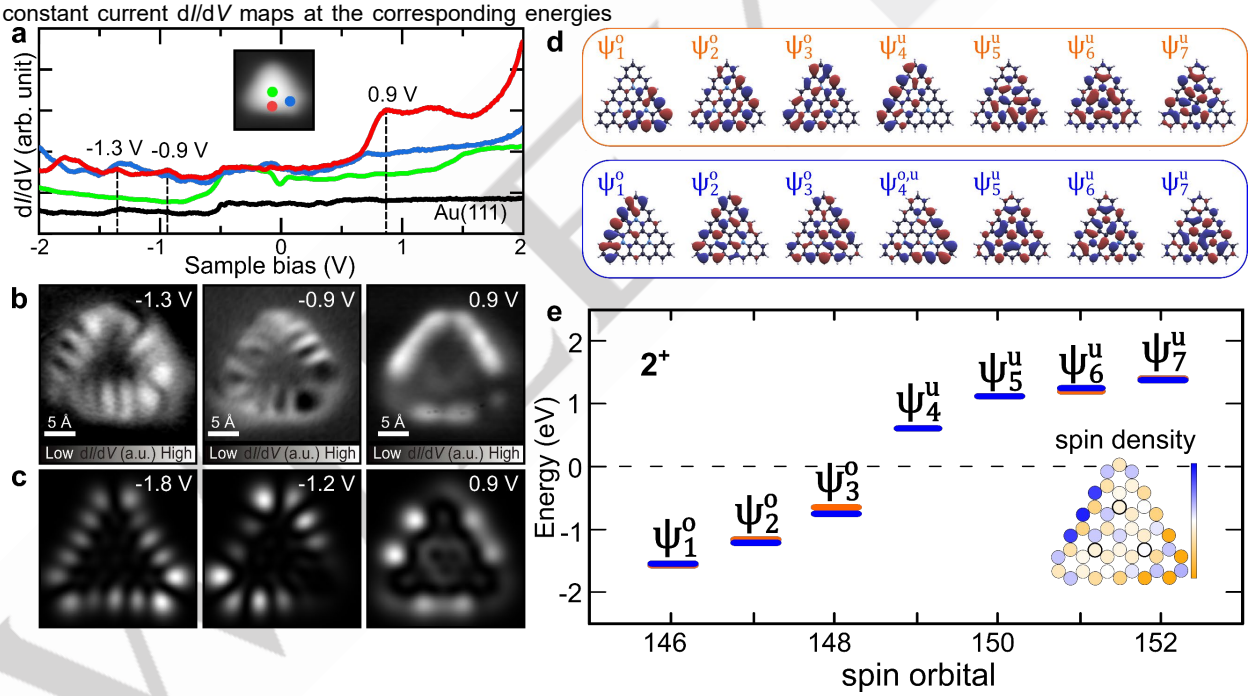

Figure 3. (a) Long-range d*I*/d*V* spectra taken at the sites of **2** marked by green, red, and blue dots in the inset. The curve in black was taken at the bar Au for a reference. V_{ac} = 10 mV. (b) Constant-current d*I*/d*V* maps of **2** taken at −1.3, −0.9, and 0.9 V with a metal tip, which was obtained by contacting to a clean gold substrate. (c) DFT simulated constant height d*I*/d*V* maps of $\mathbf{2}^+$ that best agree with the resonances observed in the experiment. (d) Spatial distribution of the wave functions of $\mathbf{2}^+$, where the ψ_4 wave function in blue is the orbital that becomes unoccupied when the system is positively charged. (e) Energy levels of $\mathbf{2}^+$ and its spin density in the inset.

In contrast to [5]triangulene[4b] (Figure 4a) and singly doped aza[5]triangulene[6b] (Figure 4b), the three extra electrons in **2** populate degenerated levels, leading to Jahn-Teller distortions and a valley-mixing of the highest occupied molecular orbital in an S = 1/2 ground state (Figure 4c). This is similar to earlier results for the smaller aza[3]triangulene.[5d] For **2**, enforcing C_3 symmetry as seen in Figure 4d leads the wave function to vanish completely at the central atoms[21]. If this restriction is removed, the distance maps reveal that the Jahn-Teller distortion is observed around the nitrogen atoms (Figure 4e), and charging the system does not

10.1002/anie.202411893

induce the C_3 symmetry (Figure 4f). The distortion also causes a distribution of the wave function over the central atoms, where **2** is then driven to an AF phase as one electron is transferred to the surface while retaining a Jahn-Teller distortion compatible to the charged system, thus leading to the C_2 symmetry of the d*I*/d*V* maps. We noticed that fixing a triplet ground state in cationic $\mathbf{2}^+$ and $\mathbf{3}^+$ brings the systems to an FM phase, increasing their total energies by 0.9 and 5.2 meV, respectively.

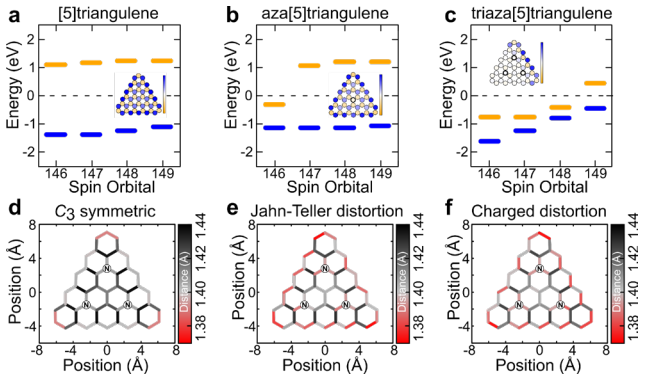

Figure 4. (a–c) Evolution of the low energy levels among [5]triangulene, aza[5]triangulene, and **2** (triaza[5]triangulene). The Insets show the spin density of each case. (d–f) Distance maps of **2** in three different scenarios: in (d) the C_3 symmetry is kept intact while in (e) and (f) the Jahn-Teller distortion is clearly seen around the nitrogen atoms for the neutral and cationic **2**, respectively.

Conclusion

We demonstrated the synthesis of triaza[5]triangulene and its derivatives via cyclodehydrogenation of triaza-precursor ion pair. BR-STM revealed their chemical structures while their open-shell singlet ground states were investigated with a combination of STS and DFT calculations. The additional π-electrons introduced by the graphitic nitrogen atoms and the charge transfer between the molecules and the substrate led to an AF alignment. We found that the azatriangulenes have a relatively high magnetic exchanging coupling strength, which is an important parameter for spin-logic operations at practical temperatures. Our results provide elementary building blocks to explore quantum magnetism and a strategy for the bottom-up synthesis of high-spin quantum nanostructures for future spintronic devices.

Acknowledgements

This work was supported by in part by Japan Society for the Promotion of Science (JSPS) KAKENHI Grant Number JP22H00285, JP22H02067, JP20H05863, and JP24K01576. The authors acknowledge funding from the Academy of Finland (project no. 346824). A.S.F. was supported by the World Premier International Research Center Initiative (WPI), MEXT, Japan. The authors acknowledge the computational resources provided by the Aalto Science-IT project and CSC, Helsinki.

Keywords: on-surface synthesis • triangulene • graphitic nitrogen • scanning tunneling microscopy/spectroscopy • density functional theory

1. a) W. Han, R. K. Kawakami, M. Gmitra, J. Fabian, *Nat. Nanotechnol.* **2014**, *9*, 794-807; b) Y. Morita, S. Suzuki, K. Sato, T. Takui, *Nat. Chem.* **2011**, *3*, 197-204; c) W. L. Wang, O. V. Yazyev, S. Meng, E. Kaxiras, *Phys. Rev. Lett.* **2009**, *102*, 157201.
2. a) J. Cai, C. A. Pignedoli, L. Talirz, P. Ruffieux, H. Söde, L. Liang, V. Meunier, R. Berger, R. Li, X. Feng, *Nat. Nanotechnol.* **2014**, *9*, 896-900; b) J. Cai, P. Ruffieux, R. Jaafar, M. Bieri, T. Braun, S. Blankenburg, M. Muoth, A. P. Seitsonen, M. Saleh, X. Feng, *Nature* **2010**, *466*, 470-473; c) Y.-C. Chen, T. Cao, C. Chen, Z. Pedramrazi, D. Haberer, D. G. De Oteyza, F. R. Fischer, S. G. Louie, M. F. Crommie, *Nat. Nanotechnol.* **2015**, *10*, 156-160; d) P. Ruffieux, S. Wang, B. Yang, C. Sánchez-Sánchez, J. Liu, T. Dienel, L. Talirz, P. Shinde, C. A. Pignedoli, D. Passerone, *Nature* **2016**, *531*, 489-492.
3. a) N. Pavlicek, A. Mistry, Z. Majzik, N. Moll, G. Meyer, D. J. Fox, L. Gross, *Nat. Nanotechnol.* **2017**, *12*, 308-311; b) S. Mishra, D. Beyer, K. Eimre, J. Liu, R. Berger, O. Groning, C. A. Pignedoli, K. Mullen, R. Fasel, X. Feng, P. Ruffieux, *J. Am. Chem. Soc.* **2019**, *141*, 10621-10625.
4. a) J. Su, J. Li, N. Guo, X. Peng, J. Yin, J. Wang, P. Lyu, Z. Luo, K. Mouthaan, J. Wu, C. Zhang, X. Wang, J. Lu, *Nat. Synth.* **2024**, 1-11; b) J. Su, M. Telychko, P. Hu, G. Macam, P. Mutombo, H. Zhang, Y. Bao, F. Cheng, Z. Huang, Z. Qiu, S. J. R. Tan, H. Lin, P. Jelínek, F. Chuang, J. Wu, J. Lu, *Sci. Adv.* **2019**, *5*, eaav7717.
5. a) E. Carbonell-Sanromà, J. Hieulle, M. Vilas-Varela, P. Brandimarte, M. Iraola, A. Barragán, J. Li, M. Abadia, M. Corso, D. Sánchez-Portal, *ACS Nano* **2017**, *11*, 7355-7361; b) S. Kawai, S. Nakatsuka, T. Hatakeyama, R. Pawlak, T. Meier, J. Tracey, E. Meyer, A. S. Foster, *Sci. Adv.* **2018**, *4*, eaar7181; c) K. Nakamura, Q.-Q. Li, O. Krejci, A. S. Foster, K. Sun, S. Kawai, S. Ito, *J. Am Chem. Soc.* **2020**, *142*, 11363-11369; d) T. Wang, A. Berdonces-Layunta, N. Friedrich, M. Vilas-Varela, J. P. Calupitan, J. I. Pascual, D. Peña, D. Casanova, M. Corso, D. G. de Oteyza, *J. Am. Chem. Soc.* **2022**, *144*, 4522-4529; e) X. Wang, J. I. Urgel, G. B. Barin, K. Eimre, M. Di Giovannantonio, A. Milani, M. Tommasini, C. A. Pignedoli, P. Ruffieux, X. Feng, *J. Am. Chem. Soc.* **2018**, *140*, 9104-9107; f) X. Wang, X. Yao, A. Narita, K. Müllen, *Acc. Chem. Res.* **2019**, *52*, 2491-2505; g) K. Sun, O. J. Silveira, S. Saito, K. Sagisaka, S. Yamaguchi, A. S. Foster, S. Kawai, *ACS Nano* **2022**, *16*, 11244-11250.
6. a) J. Lawrence, Y. He, H. Wei, J. Su, S. Song, A. W. Rodrigues, D. Miravet, P. Hawrylak, J. Zhao, J. Wu,; J. Lu, *ACS Nano* **2023**, *17*, 20237-20245; b) M. Vilas-Varela, F. Romero-Lara, A. Vegliante, J. P. Calupitan, A. Martínez, L. Meyer, U. Uriarte-Amiano, N. Friedrich, D. Wang, F. Schulz, N. E. Koval, M. E. Sandoval-Salinas, D. Casanova, M. Corso, E. Artacho, D. Peña, J. I. Pascual, *Angew. Chem. Int. Ed.* **2023**, *62*, e202307884.
7. a) L. Gross, F. Mohn, N. Moll, P. Liljeroth, G. Meyer, *Science* **2009**, *325*, 1110-1114; b) R. Temirov, S. Soubatch, O. Neucheva, A. C. Lassise, F. S. Tautz, *New J. Phys.* **2008**, *10*, 053012.
8. a) J. Li, S. Sanz, J. Castro-Esteban, M. Vilas-Varela, N. Friedrich, T. Frederiksen, D. Pena, J. I. Pascual, *Phys. Rev. Lett.* **2020**, *124*, 177201; b) J. Li, S. Sanz, M. Corso, D. J. Choi, D. Pena, T. Frederiksen, J. I. Pascual, *Nat. Commun.* **2019**, *10*, 200.
9. a) N. Pavliček, A. Mistry, Z. Majzik, N. Moll, G. Meyer, D. J. Fox, L. Gross, *Nat. Nanotechnol.* **2017**, *12*, 308-311; b) S. Mishra, S. Fatayer, S.

Fernández, K. Kaiser, D. Peña, L. Gross, *ACS Nano* **2022**, *16*, 3264-3271.
10. K. Eimre, J. I. Urgel, H. Hayashi, M. D. Giovannantonio, P. Ruffieux, S. Sato, S. Otomo, Y. Chan, N. Aratani, D. Passerone, O. Gröning, H. Yamada, R. Fasel, C. A. Pignedoli, *Nat. Commun.* **2022**, *13*, 511.
11. P. Lazar, R. Mach, M. Otyepka, *J. Phys. Chem. C* **2019**, *123*, 10695-10702.
12. T. Stuyver, B. Chen, T. Zeng, P. Geerlings, F. De Proft, R. Hoffmann, *Chem. Rev.* **2019**, *119*, 11291-11351.
13. A. Ovchinnikov, *Theor. Chim. Acta* **1978**, *47*, 297-304.
14. E. H. Lieb, *Phys. Rev. Lett.* **1989**, *62*, 1201.
15. J. Su, M. Telychko, S. Song, J. Lu, *Angew. Chem. Int. Ed.* **2020**, *59*, 7658-7668.
16. M. A. Reed, *Mater. Today* **2008**, *11*, 46-50.
17. a) Y. Zheng, C. Li, C. Xu, D. Beyer, X. Yue, Y. Zhao, G. Wang, D. Guan, Y. Li, H. Zheng, *Nat. Commun.* **2020**, *11*, 6076; b) S. Mishra, X. Yao, Q. Chen, K. Eimre, O. Gröning, R. Ortiz, M. Di Giovannantonio, J. C. Sancho-García, J. Fernández-Rossier, C. A. Pignedoli, *Nat. Chem.* **2021**, *13*, 581-586; c) Y. Zheng, C. Li, Y. Zhao, D. Beyer, G. Wang, C. Xu, X. Yue, Y. Chen, D. Guan, Y. Li, *Phy. Rev. Lett.* **2020**, *124*, 147206.
18. T. Wang, S. Sanz, J. Castro-Esteban, J. Lawrence, A. Berdonces-Layunta, M. S. G. Mohammed, M. Vilas-Varela, M. Corso, D. Pena, T. Frederiksen, D. G. de Oteyza, Graphene Nanoribbons. *Nano Lett.* **2022**, *22*, 164-171.
19. E. C. H. Wen, P. H. Jacobse, J. Jiang, Z. Wang, R. D. McCurdy, S. G. Louie, M. F. Crommie, F. R. Fischer, *J. Am. Chem. Soc.* **2022**, *144*, 13696-13703.
20. a) S. Mishra, D. Beyer, K. Eimre, R. Ortiz, J. Fernández-Rossier, R. Berger, O. Gröning, C. A. Pignedoli, R. Fasel, X. Feng, *Angew. Chem. Int. Ed.* **2020**, *132*, 12139-12145; b) S. Mishra, D. Beyer, K. Eimre, S. Kezilebieke, R. Berger, O. Gröning, C. A. Pignedoli, K. Müllen, P. Liljeroth, P. Ruffieux, *Nat. Nanotechnol.* **2020**, *15*, 22-28.
21. J. C. G. Henriques, D. Jacob, A. Molina-Sánchez, G. Catarina, A. T. Costa, J. Fernández-Rossier, *arXiv preprint* **2023**, arXiv:2312.04938.

10.1002/anie.202411893

Entry for the Table of Contents

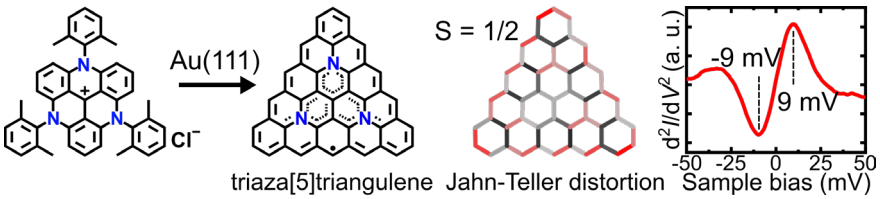

Triaza[5]triangulene, containing three graphitic nitrogen atoms, and its derivatives were successfully synthesized through cyclodehydrogenation and C–N bond cleavage from 4,8,12-Tris(2,6-dimethylphenyl)-4,8,12-triazatriangulenium on Au(111). Their chemical structures and spin states were investigated with a combination of bond-resolved STM, STS, and DFT calculations at low temperature.